



Uniform magnetization transfer in chemical exchange saturation transfer magnetic resonance imaging

Jae-Seung Lee^{1,2}, Prodromos Parasoglou¹, Ding Xia¹, Alexej Jerschow² & Ravinder R. Regatte¹

¹Quantitative Multinuclear Musculoskeletal Imaging Group, Center for Biomedical Imaging, Department of Radiology, New York University Langone Medical Center, New York, NY 10016, ²Department of Chemistry, New York University, New York, NY 10003.

SUBJECT AREAS:

CHEMICAL PHYSICS

MAGNETIC RESONANCE
IMAGING

DIAGNOSTIC MARKERS

BIOMEDICAL ENGINEERING

Received
24 January 2013

Accepted
8 April 2013

Published
23 April 2013

Correspondence and requests for materials should be addressed to A.J. (alexej.jerschow@nyu.edu) or R.R.R. (Ravinder.Regatte@nyumc.org)

The development of chemical exchange saturation transfer (CEST) has led to the establishment of new contrast mechanisms in magnetic resonance imaging, which serve as enablers for advanced molecular imaging strategies. Macromolecules in tissues and organs often give rise to broad and asymmetric exchange effects, called magnetization transfer (MT) effects, which can mask the CEST contrast of interest. We show here that the saturation of these macromolecular pools simultaneously at two distinct frequencies can level out the asymmetric MT effects, thus allowing one to isolate the CEST effects *in vivo*. For the first time, clean CEST contrast for glycosaminoglycans (gagCEST) in cartilage in the human knee joint is presented. In addition, the method allows one to clearly demarcate glycosaminoglycan measurements from cartilage and synovial fluid regions. This uniform-MT CEST methodology has wide applicability in *in vivo* molecular imaging (such as brain, skeletal muscle, etc).

Magnetic resonance imaging (MRI) has become an indispensable radiological tool for diagnosis, follow-up on treatments, clinical studies, and for drug research. As part of the molecular imaging research field, new MRI methodology has been developed towards the establishment of the *in vivo* visualization of metabolic pathways and tracking of biomarkers^{1–3}. Among these, the chemical exchange saturation transfer (CEST) technique provides powerful and flexible contrast mechanism^{4–6}, which allows the amplified detection of exchangeable proton species from biomarkers or physiologically active molecules *in vivo*. The exchangeable protons are saturated by radiofrequency (RF) irradiation, which reduces the polarization of water protons through chemical exchange. On a molecular level, chemical exchange between water and a CEST agent can occur many times during the RF irradiation. Therefore, water polarization can decrease significantly, even when the actual polarization of the CEST agent is very small.

Despite many successful demonstrations of CEST *in vivo* for a variety of endogenous and exogenous agents^{7–13}, a number of challenges persist. First, the RF irradiation saturating the exchangeable proton spins of a CEST agent often also partially saturates the water proton spins¹⁴. This effect can be minimized by taking the difference between the signal obtained after irradiating at the frequency of a CEST agent and the other signal obtained after irradiating at the mirrored frequency position on the opposite side of the water signal.

A second major difficulty is posed by the presence of water bound to macromolecules or by protons belonging to ordered structures, which may exchange spin polarizations with free water protons either chemically and/or via through-space interactions¹⁵. Such effects, commonly referred to as the magnetization transfer (MT) mechanism, may affect the water signal intensity over a broad frequency range and may lead to an inevitable interference with the desirable CEST contrast. This interference can be reduced by the difference analysis as mentioned above, but its complete removal is not trivial because the MT effect may itself be asymmetric around the water^{11,16,17}. Here, we introduce a saturation technique that can isolate genuine CEST effects by making MT effects uniform.

A weak RF irradiation at a single frequency on a system of strongly coupled nuclear spins establishes a unique internal equilibrium state between the Zeeman and dipolar orders, in which nuclear spins align respectively with the external static magnetic field and with the local magnetic field created by neighboring nuclear spins^{18,19}. If a given system is irradiated simultaneously at two distinct frequencies, however, there does not exist a common internal equilibrium state, except for the trivial state, i.e., the complete saturation of both the Zeeman and dipolar orders²⁰. Assuming that this complete saturation is achieved on a time scale much shorter than the time scale of MT effects, the MT effects can be considered uniform over a large irradiation frequency range.



The following procedure is implemented to achieve this uniform-MT (uMT) effect for the isolation of CEST contrast: First, the separation between the two RF irradiation frequency positions is fixed, for example, through a properly adjusted cosine modulation of the saturation pulse. The frequency separation should be large enough so that, at any given time, at most one CEST pool is within reach. On the other hand, the frequency separation should be smaller than the spectral range of the MT pool that one wishes to completely saturate. Since the vast majority of the proton chemical shifts lie within 6 ppm from the water resonance frequency, a good choice for the frequency separation would be 12 ppm. Second, in order to compensate for the direct water saturation by a difference analysis, one needs another experiment with the pair of irradiation frequencies exactly symmetric with respect to the water resonance frequency (Fig. 1a). Taking the difference between the two experiments can then reveal pure CEST effects. Recently, this uMT CEST scheme has been implemented on gelatin solutions and cartilage tissue specimens²¹.

Results

Numerical simulation. In order to scan the frequency range for exchangeable sites as well as to perform B_0 inhomogeneity correction²², the water signal intensity is usually measured as a function of the frequency offset of the RF irradiation (Z spectrum)²³. Our uMT CEST method is performed in the same way as the conventional CEST method, except that the saturating RF irradiation is a cosine-modulated pulse with a predetermined modulation frequency (f_m in Fig. 1a). The Z spectrum is recorded

against the frequency offset (f_0 in Fig. 1a) of the cosine-modulated pulse. The uMT CEST method can be easily distinguished from the conventional CEST method by the number of dips in the Z spectrum (Fig. 1b) since the direct water saturation happens twice in the uMT CEST method. The difference analysis on a Z spectrum produces the so-called MT asymmetry curve (Figs. 1c and 1d)²⁴. The uMT CEST method can also be easily distinguished by the positive and negative MT asymmetry peaks appearing around the predetermined modulation frequency (Fig. 1d). The signs of those peaks arise from the way the Z spectrum from the uMT method is plotted, as seen in Fig. 1b. In the conventional CEST method, the MT asymmetry peak may contain both CEST and asymmetric MT effects together, indicated respectively as red and blue dashed lines in Fig. 1c. In the uMT CEST method, the negative MT asymmetry peak at the smaller frequency offset may be free from the MT effects, while the positive peak at the larger frequency offset contains both the CEST and MT effects (Fig. 1d). In this simulation, the spectral range of the MT pool was such that the MT effect became independent of the frequency offset when the frequency offset was small. When the frequency offset was large, the condition of the simultaneous irradiation at two distinct frequencies was not met because one of the two frequencies was out of the spectral range of the MT pool, which leads to asymmetric MT interference with the positive peak. One key indication for the success of uMT in the isolation of the CEST effect may be evidenced by the flatness of the Z spectrum or close-to-zero MT asymmetry around the zero frequency offset (Supplementary Fig. S1).

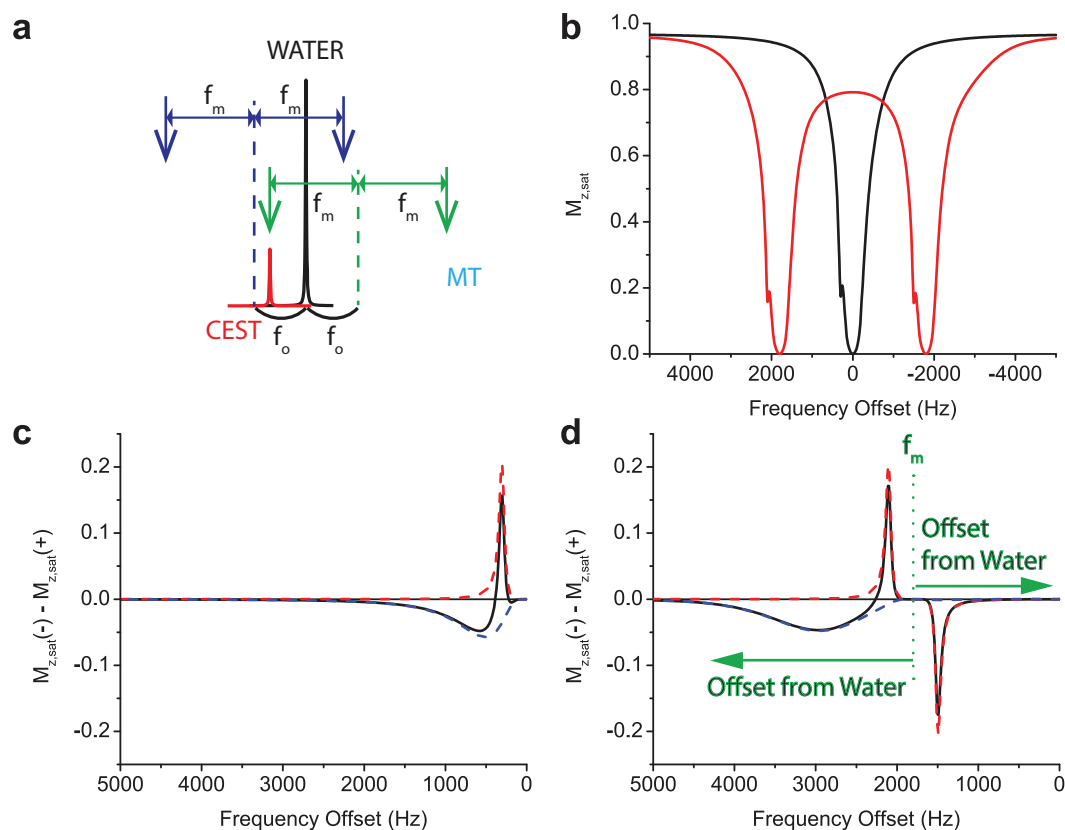


Figure 1 | Comparison between conventional and uMT CEST methods. (a), Schematic of uMT CEST experiments. Using a pair of simultaneous two-frequency RF irradiation symmetric with respect to the water resonance frequency, CEST effects can be isolated. The frequency separation between the two frequency components and their average frequency offset are given as $2 \times f_m$ and f_0 , respectively. (b), Simulated Z spectra (conventional – black; uMT – red). (c), In the conventional CEST method, the CEST peak is affected by asymmetric MT effects (simulations including both CEST and MT processes – black, only the CEST process – red, and only the MT process – blue). (d), In the uMT CEST method, the negative peak appearing close to the zero frequency offset may count only the CEST effect because the MT effects become uniform.

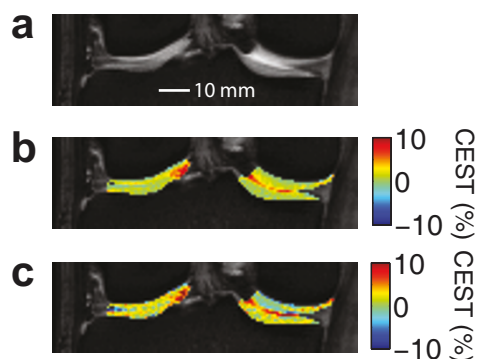


Figure 2 | gagCEST contrast maps. (a), Anatomical reference image from the right knee of a healthy volunteer. (b), Conventional gagCEST contrast map, superimposed onto an anatomical reference image, shows the integrated MT asymmetry per Hz over the frequency offsets between 0 Hz and 600 Hz. (c), uMT gagCEST contrast map, superimposed onto an anatomical reference image, shows the negated integrated MT asymmetry over the frequency offset between 1200 Hz and 1800 Hz. The gagCEST contrast maps were B_0 -corrected. The gagCEST contrast maps for all five volunteers are shown in Supplementary Fig. S2.

In-vivo human knee studies. The conventional and uMT gagCEST contrast maps from a knee of a healthy human subject are shown in Fig. 2 (Supplementary Fig. S2 shows the gagCEST contrast maps from all the human subjects). In order to check whether the uMT method reduced asymmetric MT effects, we tried to segment the regions depending on MT effects. When the frequency offset of the cosine-modulated saturation is zero, the two irradiation frequency positions (± 6 ppm) are sufficiently far from the resonance frequencies of the water and gagCEST pools, so that only the MT effects contribute to the decrease in the water signal intensity. MT contrast may then be quantified accurately by the relative decrease in the water signal intensity by the simultaneous two-frequency RF irradiation at the zero frequency offset. The MT contrast maps (Fig. 3a) revealed regions with weaker MT effects, which we suspect are due to synovial fluid. Segments with larger MT effects

(>50%) may be safely assigned to cartilage tissue and are expected to have substantial asymmetric MT effects, as observed in cartilage tissue specimens²⁰. These larger-MT regions were chosen to obtain the averaged Z spectra and MT asymmetry curves for further comparison between the conventional and uMT gagCEST results. The MT asymmetry curves from the lateral and medial femorotibial cartilage (Figs. 3b and 3c) clearly show that the MT asymmetry between the frequency offsets 1200 Hz and 1800 Hz returns to the zero baseline with the uMT method, thus indicating uniform MT effects (The averaged MT asymmetry curves from the lateral and medial femorotibial cartilage of all the human subjects are presented in Supplementary Fig. S3). In Fig. 4, the integrated asymmetric MT effects from five subjects are presented together with the averages and standard deviations. The variability of the integrated asymmetric MT effects is much smaller with the uMT CEST method, indicating that the asymmetric MT effects are invariably reduced.

In addition, it has been observed that the weaker-MT segments correspond to the regions with the stronger gagCEST effects, as seen in Figs. 2b, 2c, and 3a (see also Supplementary Fig. S4). While meniscus has very low GAG content (~ 1 –2%) compared with 5–6% in cartilage, synovial fluid has hyaluronan (HA), which may be the origin of the stronger gagCEST effects. In any case, our uMT CEST method may provide an integrated means to separately monitor molecules in different environments. The stronger and more uniform contrast of the uMT method can provide a more reliable demarcation between the tissues than conventional CEST and MT measurements (Supplementary Fig. S5).

Discussion

The gagCEST effects discussed above are attributed to the exchangeable protons in hydroxyl ($-\text{OH}$) groups^{7,25}. An additional MT asymmetry peak has been observed in all subjects, as indicated by asterisks in Figs. 3b and 3c, which to the best of our knowledge has never been observed in CS solutions or *ex vivo* specimens. Candidates for this effect are the CEST effects due to the exchangeable protons in amide ($-\text{NH}$) groups of GAGs and nuclear Overhauser effects (NOE) due to nonexchangeable protons in GAGs⁷. The averaged Z spectra

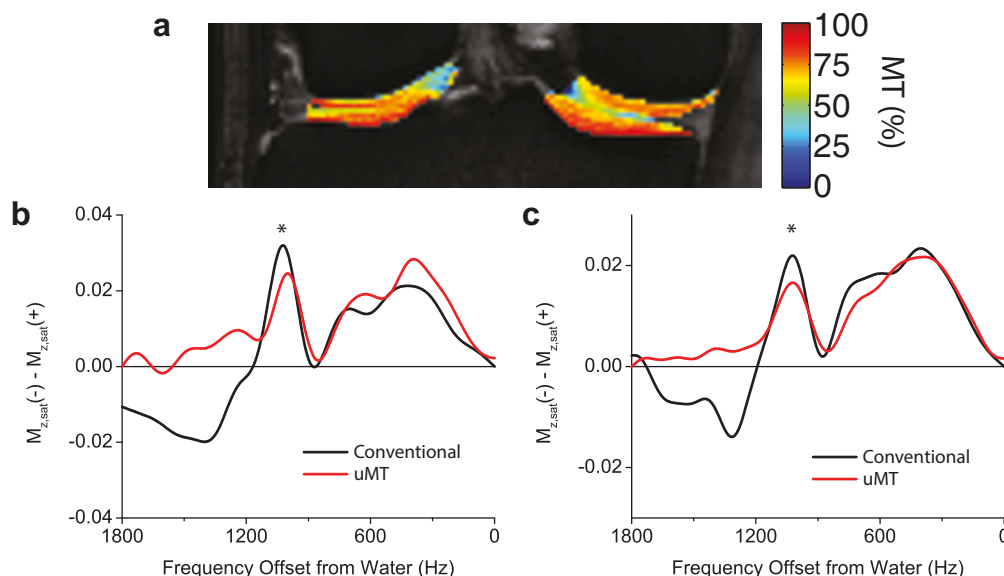


Figure 3 | Removal of asymmetric MT effects from the MT asymmetry. (a), A uMT contrast map from the right knee of a volunteer, superimposed onto the anatomical reference image. MT asymmetry curves averaged over the segments on the lateral (b) and medial (c) femorotibial cartilage, which consist of the pixels with the uMT contrast more than 50%. Black and red lines are MT asymmetry curves, respectively, from the conventional and uMT CEST acquisitions. The MT asymmetry curves from the uMT CEST method were inverted and shifted for ease of comparison with the conventional CEST method.

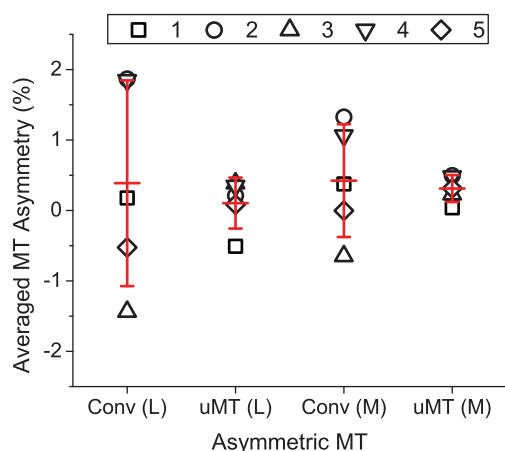


Figure 4 | Asymmetric MT effects from five human subjects. ‘Conv’ and ‘uMT’ refer to the data from the conventional and uMT CEST experiments, respectively. ‘L’ and ‘M’ indicate the segments on the lateral and medial cartilage, respectively, as shown in Fig. 3a. The red lines represent the averages and standard deviations over the subjects. The standard deviations with the uMT method are smaller by a factor of about 4 than those with the conventional method.

(Supplementary Fig. S6) revealed a kink near NOE sites, which was observed even in the weaker-MT segments. This observation may contradict earlier findings^{7,26}, but the uMT method would allow us to further investigate this MT asymmetry peak more accurately than previously possible.

A cosine-modulated pulse splits its RF power equally into two frequencies. By setting the power of the cosine-modulated Gaussian pulse in the uMT method to double the power of the Gaussian pulse in the conventional method, the capability of detecting CEST effects are presumed to be same for both the conventional and uMT CEST methods. Any B_0 and B_1 field inhomogeneities would affect both the methods in a similar way, except that the doubled RF power of the saturating RF irradiation with the uMT method could cause more RF heating, which could increase the temperature of tissue and affect some conditions for CEST effects such as exchange rates, chemical shifts, and relaxation times. On the other hand, the uMT method allows one to suppress asymmetric MT over a large range of offset frequencies and power levels^{20,21}, which indicates that it could also perform better in additional B_1 correction protocols that were designed for CEST^{27,28}. NOE affects both the conventional and uMT methods equally, except in cases where there might be accidental simultaneous saturation of CEST and NOE sites in the uMT method. While the uMT method needs to cover a larger range of the frequency offsets of the saturating RF irradiation, useful information such as a B_0 maps and uMT contrast can be extracted without any additional experiments.

The results presented herein suggest that asymmetric MT effects, which often interfere with CEST measurements, can be eliminated, and clean MT-free CEST contrast can be obtained. We demonstrate particular implementations relevant for gagCEST *in vivo* in the human knee, but the procedure is general for all CEST-type experiments. For the human knee, the uMT CEST method produces a uMT contrast map that seems to allow separating two types of GAGs in a human knee joint, CS in cartilage tissue and HA in synovial fluid, both of which have been known to correlate with the development of joint diseases, for example, osteoarthritis^{29,30}.

CEST MRI may measure GAG concentrations more directly compared with other existing methods³¹ that are based on measuring the fixed charge density of GAGs, such as delayed gadolinium-enhanced MRI of cartilage (dGEMRIC) and fluid-suppressed sodium inversion recovery MRI (hardware modifications), and may be safer than dGEMRIC because it does not require any exogenous contrast

agents. It generally also requires much less power than $T_{1\rho}$ MRI. Although more investigations are required to validate these capabilities, the uMT CEST method has a potential to become an invaluable molecular imaging tool to study the role of GAGs in the degeneration of knee joints and to better diagnose osteoarthritis.

Most importantly, up to now, *in vivo* CEST imaging has had to contend with underlying MT asymmetries which were often hard to distinguish from genuine CEST or NOE effects. Although a recent technique called FLEX³² has some capability of distinguishing between these mechanisms, it currently requires a significant overhead. The uMT method, by contrast, directly disentangles and isolates these two effects. As a result, both clean CEST and MT contrast images can be obtained as demonstrated herein.

Methods

Simulation. A three-pool model was set up based on Provotorov’s partial saturation theory^{20,21}. There are water, MT, and CEST pools, the concentrations of which are set to be 0.97, 0.02, and 0.01, respectively. For the water pool, the longitudinal and transverse relaxation times are respectively 5 sec and 1 sec, and the line shape is given as $g_{\text{water}}(\Delta) = (T_2/\pi)/(1 + 4\Delta^2T_2^2)$. For the MT pool, the longitudinal and dipolar relaxation times are respectively 5 sec and 1 sec, and the line shape is given as $g_{\text{MT}}(\Delta) = \exp[-4\pi^2(\Delta + 300 \text{ Hz})^2/(6\omega_{\text{loc}}^2)]/[(6\pi)^{1/2}\omega_{\text{loc}}]$, with the dipolar local field $\omega_{\text{loc}}/2\pi = 1000 \text{ Hz}$. For the CEST pool, the longitudinal and transverse relaxation times are the same as for the water pool, and the line shape is given as $g_{\text{CEST}}(\Delta) = (T_2/\pi)/(1 + 4(\Delta - 300 \text{ Hz})^2T_2^2)$. The strength and duration of the saturating field are given as $\omega_1/2\pi = 100 \text{ Hz}$ and 1 sec, respectively, and the distance between the frequency positions of two simultaneous RF irradiations is set to be 3600 Hz. The exchange rates are given as $k_{\text{water} \rightarrow \text{CEST}} = 1 \text{ s}^{-1}$, $k_{\text{water} \rightarrow \text{MT}} = 0.2 \text{ s}^{-1}$, $k_{\text{CEST} \rightarrow \text{water}} = 97 \text{ s}^{-1}$, $k_{\text{MT} \rightarrow \text{water}} = 9.7 \text{ s}^{-1}$, and $k_{\text{MT} \rightarrow \text{CEST}} = k_{\text{CEST} \rightarrow \text{MT}} = 0 \text{ s}^{-1}$. The z-component of the magnetization of the water pool was numerically calculated by using the ode45 function in MATLAB, and then the MT asymmetry curve was obtained. In order to see how each of the CEST and MT effects contributes to the MT asymmetry, only the irrelevant exchange rates were set to zero without changing other parameters.

MRI human subjects. After approval from the Institutional Review Board of the New York University Medical Center and signed informed consent, the right knee joints of five healthy volunteers (all male, mean age 31.0 ± 4.3 years) were investigated.

MRI hardware. The MRI experiments were performed on a 7T whole-body Siemens scanner (Siemens, Erlangen, Germany) with a 28-element 7T knee coil array (Quality Electrodynamics, Mayfield Village, OH).

MRI experiments. The study protocol consisted of a localizer, uMT CEST acquisition, conventional CEST acquisition, and WASSR²² acquisition. The schemes of the MRI pulses sequences are shown in Supplementary Fig. S7. For the signal acquisition, a segmented GRE acquisition with centric phase encoding order was used. For the GRE sequence, Flip Angle = 10° , TR = 24 ms, TE = 3.5 ms, dwell time = 15 μs , FOV = $160 \times 160 \text{ mm}^2$, slice thickness = 5 mm, matrix size = 192×192 . The image is acquired in two segments. For the off-resonance presaturation, a train of 10 Gaussian and cosine-modulated Gaussian pulses were used in the conventional and uMT CEST experiments, respectively, each 100 ms long, with their frequency offsets being varied from -3600 Hz to 3600 Hz with a step size of 100 Hz. Their nominal flip angles were 1800° ($B_{1,\text{rms}} = 1.7 \mu\text{T}$) and 3600° ($B_{1,\text{rms}} = 2.4 \mu\text{T}$) for the conventional and uMT CEST experiments, respectively. The modulation frequency for the cosine-modulated Gaussian pulse was 1.8 kHz. For the WASSR acquisition, two 100 ms-long 180° gauss pulses were used during the pre-saturation, and the frequency offset was varied from -720 Hz to 720 Hz with a step size of 20 Hz.

Data analysis. All the image reconstruction and data processing were performed using MATLAB. Each image was reconstructed using a sum-of-squares combination. The following data processing was performed on the pixels in the selected segments (Supplementary Fig. S8). From the WASSR and uMT CEST acquisitions, B_0 maps were reconstructed pixel-wise in terms of frequency values by locating the minima of the interpolated Z spectra, which were estimated at every 1 Hz by using the cubic spline interpolation. From the WASSR acquisition, each interpolated Z spectrum has one minimum, which is taken as B_0 . From the uMT CEST acquisition, each interpolated Z spectrum should have two minima around $\pm 1800 \text{ Hz}$. The average of the frequency positions of the two minima is taken as B_0 . The gagCEST contrast was obtained as follows: The Z spectra were reconstructed pixel-wise, interpolated by using a cubic spline interpolation, and shifted by the corresponding B_0 values. The MT asymmetry was taken by subtracting the value at the positive offsets from the value at the corresponding negative offsets and dividing by the signal intensity from a reference image collected without pre-saturation and integrated over the frequency offsets between 0 Hz and 600 Hz for the conventional gagCEST and between 1200 Hz to 1800 Hz for the uMT gagCEST, which was then negated. While the B_0 inhomogeneity was corrected with the B_0 map estimated from the same data set for the uMT gagCEST contrast, it was performed with the B_0 map from the WASSR acquisition for the conventional gagCEST. The Z spectrum averaged over a chosen



segment with larger MT effects was obtained by first summing the signal intensities inside the segments from the B_0 -corrected data, and then divided by the signal intensity summed over the segment from the reference image. The MT asymmetry curves between 0 Hz and 1800 Hz from the uMT method were inverted and reversed for ease of comparison with those from the conventional method. To compare the variability in the asymmetric MT effects through the subjects, the integrations were performed on the MT asymmetry curves from the larger-MT segments in the lateral and medial femorotibial cartilage, over the frequency offsets from 1200 Hz to 1800 Hz, and normalized per Hz.

- Ottobri, L., Ciana, P., Biserni, A., Lucignani, G. & Maggi, A. Molecular imaging: A new way to study molecular processes in vivo. *Mol. Cell. Endocrinol.* **246**, 69–75 (2006).
- Massoud, T. F. & Gambhir, S. S. Molecular imaging in living subjects: seeing fundamental biological processes in a new light. *Genes Dev.* **17**, 545–580 (2003).
- Jaffer, F. A. & Weissleder, R. Molecular Imaging in the Clinical Arena. *JAMA* **293**, 855–862 (2005).
- Zhou, J. & van Zijl, P. C. M. Chemical exchange saturation transfer imaging and spectroscopy. *Prog. NMR Spectsc.* **48**, 109–136 (2006).
- De Leon-Rodriguez, L. M. *et al.* Responsive MRI Agents for Sensing Metabolism in Vivo. *Acc. Chem. Res.* **42**, 948–957 (2009).
- van Zijl, P. C. M. & Yadav, N. N. Chemical Exchange Saturation Transfer (CEST): What is in a Name and What Isn't? *Magn. Reson. Med.* **65**, 927–948 (2011).
- Ling, W., Regatte, R. R., Navon, G. & Jerschow, A. Assessment of glycosaminoglycan concentration in vivo by chemical exchange-dependent saturation transfer (gagCEST). *Proc. Natl. Acad. Sci. U.S.A.* **105**, 2266–2270 (2008).
- Zhou, J., Lal, B., Wilson, D. A., Larter, J. & van Zijl, P. C. M. Amide Proton Transfer (APT) Contrast for Imaging of Brain Tumors. *Magn. Reson. Med.* **50**, 1120–1126 (2003).
- Aime, S., Delli Castelli, D. & Terreno, E. Highly Sensitive MRI Chemical Exchange Saturation Transfer Agents Using Liposomes. *Angew. Chem. Int. Ed.* **44**, 5513–5515 (2005).
- Schroder, L., Lowery, T. J., Hilty, C., Wemmer, D. E. & Pines, A. Molecular Imaging Using a Targeted Magnetic Resonance Hyperpolarized Biosensor. *Science* **314**, 446–449 (2006).
- van Zijl, P. C. M., Jones, C. K., Ren, J., Malloy, C. R. & Sherry, A. D. MRI detection of glycogen in vivo by using chemical exchange saturation transfer imaging (glycoCEST). *Proc. Natl. Acad. Sci. USA* **104**, 4359–4364 (2007).
- Haris, M., Cai, K., Singh, A., Hariharan, H. & Reddy, R. In vivo mapping of brain myo-inositol. *NeuroImage* **54**, 2079–2085 (2011).
- Cai, K. *et al.* Magnetic resonance imaging of glutamate. *Nat Med* **18**, 302–306 (2012).
- Zhou, J., Payen, J.-F., Wilson, D. A., Traystman, R. J. & van Zijl, P. C. M. Using the amide proton signals of intracellular proteins and peptides to detect pH effects in MRI. *Nat. Med.* **9**, 1085–1090 (2003).
- Henkelman, R. M., Stanisz, G. J. & Graham, S. J. Magnetization transfer in MRI: a review. *NMR Biomed.* **14**, 57–64 (2001).
- Hua, J. *et al.* Quantitative Description of the Asymmetry in Magnetization Transfer Effects Around the Water Resonance in the Human Brain. *Magn. Reson. Med.* **58**, 786–793 (2007).
- Ng, M.-C., Hua, J., Hu, Y., Luk, K. D. & Lam, E. Y. Magnetization Transfer (MT) Asymmetry Around the Water Resonance in Human Cervical Spinal Cord. *J. Magn. Reson. Imaging* **29**, 523–528 (2009).
- Provotorov, B. N. Magnetic-resonance saturation in crystals. *Zh. Eksperim. i Teor. Fiz.* **41**, 1582–1591 (1961).
- Goldman, M. *Spin Temperature and Nuclear Magnetic Resonance in Solids* (Clarendon, Oxford, 1970).
- Lee, J.-S., Khitrin, A. K., Regatte, R. R. & Jerschow, A. Uniform saturation of a strongly coupled spin system by two-frequency irradiation. *J. Chem. Phys.* **134**, 234504 (2011).
- Lee, J.-S., Regatte, R. R. & Jerschow, A. Isolating chemical exchange saturation transfer contrast from magnetization transfer asymmetry under two-frequency irradiation. *J. Magn. Reson.* **215**, 56–63 (2012).
- Kim, M., Gillen, J., Landman, B. A., Zhou, J. & van Zijl, P. C. M. Water Saturation Shift Referencing (WASSR) for Chemical Exchange Saturation Transfer (CEST) Experiments. *Magn. Reson. Med.* **61**, 1441–1450 (2009).
- Bryant, R. G. The dynamics of water-protein interactions. *Annu. Rev. Biophys. Biomol. Struct.* **25**, 29–53 (1996).
- Guivel-Scharen, V., Sinnwell, T., Wolff, S. D. & Balaban, R. S. Detection of Proton Chemical Exchange between Metabolites and Water in Biological Tissues. *J. Magn. Reson.* **133**, 36–45 (1998).
- Singh, A. *et al.* Chemical Exchange Saturation Transfer Magnetic Resonance Imaging of Human Knee Cartilage at 3 T And 7 T. *Magn. Reson. Med.* **68**, 588–594 (2012).
- Jia, G. *et al.* Quantitative assessment of mobile protein levels in human knee synovial fluid: feasibility of chemical exchange saturation transfer (proteinCEST) MRI of osteoarthritis. *Magn. Reson. Imaging* **29**, 335–341 (2011).
- Sun, P. Z., Farrar, C. T. & Sorensen, A. G. Correction for artifacts induced by B_0 and B_1 field inhomogeneities in pH-sensitive chemical exchange saturation transfer (CEST) imaging. *Magn. Reson. Med.* **58**, 1207–1215 (2007).
- Singh, A., Cai, K., Haris, M., Hariharan, H. & Reddy, R. On B_1 inhomogeneity correction of in vivo human brain glutamate chemical exchange saturation transfer contrast at 7T. *Magn. Reson. Med.* **69**, 818–824 (2013).
- Bollet, A. J., Handy, J. R. & Sturgill, B. C. Chondroitin sulfate concentration and protein-polysaccharide composition of articular cartilage in osteoarthritis. *J. Clin. Invest.* **42**, 853–859 (1963).
- Praest, B. M., Greiling, H. & Kock, R. Assay of synovial fluid parameters: hyaluronan concentration as a potential marker for joint diseases. *Clin. Chim. Acta* **266**, 117–128 (1997).
- Crema, M. D. *et al.* Articular cartilage in the knee: current MR imaging techniques and applications in clinical practice and research. *Radiographics* **31**, 37–61 (2011).
- Lin, C.-Y. *et al.* Using Frequency-Labeled Exchange Transfer to Separate Out Conventional Magnetization Transfer Effects From Exchange Transfer Effects When Detecting ParaCEST Agents. *Magn. Reson. Med.* **67**, 906–911 (2012).

Acknowledgements

We acknowledge financial support from the National Institutes of Health (grants K25AR060269, R21AR05724, R01AR053133, R01AR056260 and R01AR060238) and from the US National Science Foundation (grant CHE0957586).

Author contributions

J.-S.L., P.P. and R.R.R. designed the experiment. J.-S.L., P.P., D.X. and R.R.R. coordinated/performed experiments and analyzed the data. J.-S.L., P.P., A.J. and R.R.R. interpreted the results. J.-S.L. performed simulation. All authors contributed to the final manuscript.

Additional information

Supplementary information accompanies this paper at <http://www.nature.com/scientificreports>

Competing financial interests: The authors declare no competing financial interests.

License: This work is licensed under a Creative Commons

Attribution-NonCommercial-NoDerivs 3.0 Unported License. To view a copy of this license, visit <http://creativecommons.org/licenses/by-nc-nd/3.0/>

How to cite this article: Lee, J.-S., Parasoglou, P., Xia, D., Jerschow, A. & Regatte, R.R. Uniform magnetization transfer in chemical exchange saturation transfer magnetic resonance imaging. *Sci. Rep.* **3**, 1707; DOI:10.1038/srep01707 (2013).



SUBJECT AREAS:
 CHEMICAL PHYSICS
 MAGNETIC RESONANCE
 IMAGING
 DIAGNOSTIC MARKERS
 BIOMEDICAL ENGINEERING

ERRATUM: Uniform magnetization transfer in chemical exchange saturation transfer magnetic resonance imaging

Jae-Seung Lee, Prodromos Parasoglou, Ding Xia, Alexej Jerschow & Ravinder R. Regatte

The baseline and the magnetization transfer (MT) line were omitted from Figure 1a during the typesetting of the Article. The correct Figure 1 appears below.

SCIENTIFIC REPORTS:
 3 : 1707
 DOI: 10.1038/srep01707
 (2013)

Published:
 23 April 2013

Updated:
 22 November 2013

